remote sensing

MDPI

Article

Modeling of Alpine Grassland Cover Based on Unmanned Aerial Vehicle Technology and Multi-Factor Methods: A Case Study in the East of Tibetan Plateau, China

Baoping Meng [1,2], Jinlong Gao [1,2], Tiangang Liang [1,2,*], Xia Cui [3], Jing Ge [1,2], Jianpeng Yin [1,2], Qisheng Feng [1,2] and Hongjie Xie [4]

1 State Key Laboratory of Grassland Agro-ecosystems, College of Pastoral Agriculture Science and Technology, Lanzhou University, Lanzhou 730020, China; mengbp09@lzu.edu.cn (B.M.); rslabjinlong@163.com (J.G.); gej12@lzu.edu.cn (J.G.); yinjp2013@lzu.edu.cn (J.Y.); fengqsh@lzu.edu.cn (Q.F.)

2 Key Laboratory of Grassland Livestock Industry Innovation, Ministry of Agriculture, Lanzhou University, Lanzhou 730020, China

3 Key Laboratory of Western China's Environmental Systems (Ministry of Education), College of Earth and Environmental Sciences, Lanzhou University, Lanzhou 730000, China; xiacui@lzu.edu.cn

4 Laboratory for Remote Sensing and Geoinformatics, University of Texas at San Antonio, San Antonio, TX 78249, USA; hongjie.xie@utsa.edu

* Correspondence: tgliang@lzu.edu.cn; Tel.: +86-931-981-5306; Fax: +86-931-891-0979

Received: 10 January 2018; Accepted: 16 February 2018; Published: 21 February 2018

Abstract: Grassland cover and its temporal changes are key parameters in the estimation and monitoring of ecosystems and their functions, especially via remote sensing. However, the most suitable model for estimating grassland cover and the differences between models has rarely been studied in alpine meadow grasslands. In this study, field measurements of grassland cover in Gannan Prefecture, from 2014 to 2016, were acquired using unmanned aerial vehicle (UAV) technology. Single-factor parametric and multi-factor parametric/non-parametric cover inversion models were then constructed based on 14 factors related to grassland cover, and the dynamic variation of the annual maximum cover was analyzed. The results show that (1) nine out of 14 factors (longitude, latitude, elevation, the concentrations of clay and sand in the surface and bottom soils, temperature, precipitation, enhanced vegetation index (EVI) and normalized difference vegetation index (NDVI)) exert a significant effect on grassland cover in the study area. The logarithmic model based on EVI presents the best performance, with an R^2 and RMSE of 0.52 and 16.96%, respectively. Single-factor grassland cover inversion models account for only 1–49% of the variation in cover during the growth season. (2) The optimum grassland cover inversion model is the artificial neural network (BP-ANN), with an R^2 and RMSE of 0.72 and 13.38%, and SDs of 0.062% and 1.615%, respectively. Both the accuracy and the stability of the BP-ANN model are higher than those of the single-factor parametric models and multi-factor parametric/non-parametric models. (3) The annual maximum cover in Gannan Prefecture presents an increasing trend over 60.60% of the entire study area, while 36.54% is presently stable and 2.86% exhibits a decreasing trend.

Keywords: grassland cover; unmanned aerial vehicle; multi-factor; inversion model; dynamic variation

1. Introduction

Vegetation cover is a direct quantitative index, reflecting vegetation growth conditions, and is a key parameter in the estimation and monitoring of ecosystems and their functions, especially when remote-sensing methods are used, and particularly on the expansive grasslands of the Tibetan

Plateau [1]. Important cover-related parameters and functions include aboveground biomass [2–5], evapotranspiration [6] and leaf area index [7]. In addition, plant coverage and its changes over time have been directly used as indicators of grassland degradation, soil erosion [8–10] and desertification [11]. Under actual production conditions, changes in grassland cover can reveal over-grazing, aid in the monitoring of land use (e.g., changes between grassland and farmland) [12], and provide an early warning of grassland degradation. Therefore, accurate estimation of cover has a significant impact on our understanding of the existing and changing processes involved in regional ecology, and could support policy decision-making by local governments.

There are many traditional methods for observing grassland cover, and these methods can be divided into three categories based on the principle measurement involved. (1) Visual estimation methods, in which the results are obtained by a specialist through visual measurements, are the simplest of these methods. The disadvantages of visual estimation methods are that subjectivity can be high and accuracy cannot be evaluated [13,14]. (2) Sampling methods, including quadrat sampling, belt transect sampling, point count, and shadow methods, are based on a quadrat (50 cm $\times$ 50 cm or 1 m $\times$ 1 m in grassland), and their accuracy is based on the number of quadrats examined and on a logical sampling strategy. These methods require considerable time and energy to obtain high accuracy [4]. Finally, (3) instrument measurement methods include the spatial quantum sensor (SQS), traversing quantum sell (TQS) [15] and photographic methods. Although SQS and TQS can increase accuracy in the measurement of grassland cover, these methods are not suitable for field observations because of the inconvenience associated with the equipment involved. The photographic method is the most popular method for field observations due to its convenient operation and fast, accurate cover acquisition [14]. However, the aforementioned methods cannot effectively address the spatial matching between sampling sites and remote-sensing pixels, and the sampling sites are not sufficiently representative of a complex natural grassland pasture with strong spatial heterogeneity. The use of an unmanned aerial vehicle (UAV) is one possible solution to this problem [16]. Recently, UAVs have presented great potential for use by ecologists and have been evaluated as a valuable tool to replace traditional methods [16–20].

Remote sensing is the only available tool for assessing and monitoring grassland cover in the poor environment and enormous spatial extent of the Tibetan Plateau [1]. Most grassland cover estimation and monitoring are based on the normalized difference vegetation index (NDVI) and the enhanced vegetation index (EVI), which are determined using moderate-resolution imaging spectroradiometer (MODIS) images due to their high temporal resolution (daily) and wide spatial coverage (2330 km) [21]. For models estimating grassland cover, some studies use linear spectral unmixing [22,23], and most studies use regression analysis. Recently, a more advanced multivariate method that includes both parametric and non-parametric regression (e.g., multivariate linear regression, nonlinear regression and machine-learning algorithms) has been employed [3,24]. The variables used in cover inversion models are not limited to remote-sensing vegetation indices, and there is a strong correlation between grassland cover and factors related to geographical location, topographical and meteorological data, and so on [2,25]. However, few studies have addressed the question of which method is most suitable for estimating grassland cover, or determined the differences between the models, particularly in Gannan Prefecture on the Tibetan Plateau. Consequently, reliable, area-wide information on grassland cover and its changes over time has not been acquired to date.

In this study, considering the factors discussed above, a UAV is used to observe field grassland cover, replacing the traditional sampling method, and a region of alpine meadow grassland (Gannan Prefecture) on the Tibetan Plateau is studied to investigate the following: (1) the influence of the use of different methods on grassland cover estimation error by comparing and analyzing cover estimation models and their accuracy, based on single-factor parametric and multi-factor parametric/non-parametric models and (2) the applicability of present cover models and the causes of error in different models. Based on the research results obtained, we propose a method for generating

a growth season plant cover dataset for the grasslands of Gannan Prefecture from 2000 to 2016 and analyze the dynamic variation in grassland cover.

2. Data and Methods

2.1. Study Area

Gannan Prefecture (33°06′–35°44′N, 100°46′–104°44′E) is located on the Northeastern Qinghai–Tibet Plateau (Figure 1) and has a mean elevation greater than 3000 m [26]. The region has a continental plateau climate: the weather is typically cold and damp, and annual precipitation varies from 400 to 800 mm. Mean annual temperatures range from 1–3 °C, average temperatures only rise above 10 °C during two months of the year, and the annual mean sunshine duration is 2000–2400 h [27,28]. Grassland plays an important role in livestock and animal production in Gannan Prefecture because of its vast area (grassland area of 2.72×10^6 ha, accounting for 70.28% of the total prefecture area, with usable grassland of 2.57×10^6 ha) [29]. The major types of grassland are alpine meadow and alpine scrub meadow, and five other grassland types occupy much smaller areas; the latter include temperate meadow grasslands, temperate steppes, lower-flat meadows, warm-temperate tussocks and marshes.

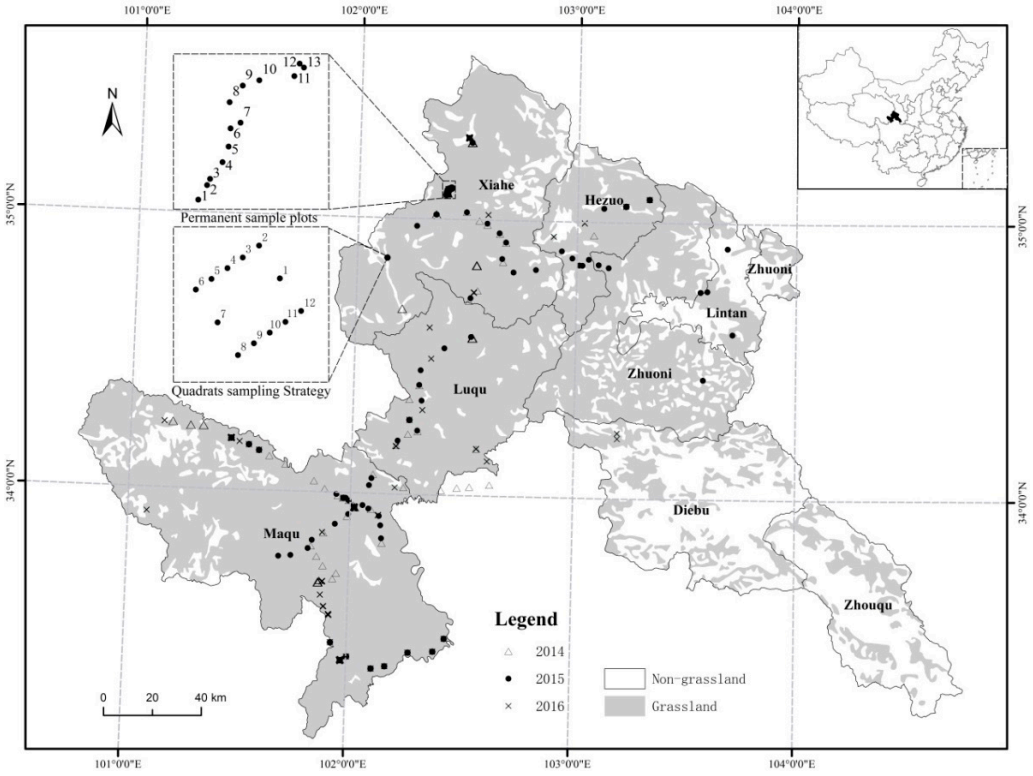

Figure 1. Location of the observation sites in the pastoral area of Gannan Prefecture, China.

2.2. Sampling Strategy and Data Collection

The evaluated grassland cover data includes two components: permanent plot data and random plot data. The permanent plot study area is located in the Yangji Community (land area of 272.26×10^4 ha) in Sangke Town in Xiahe County, Gannan Prefecture. The grassland type in this area is alpine meadow, which is the most representative grassland type in Gannan. A total of 13 sample plots (250 m × 250 m in land area) were established inside the permanent plot area (Figure 1). The locations of the 13 plots were selected based on the following criteria: (1) the growth status of the grassland was relatively uniform and spatially representative and (2) each sample plot corresponded to one

MODIS pixel. During the grassland growth seasons from 2014 to 2016, observations were performed approximately every 10 days, and 18 field investigations were conducted over the three-year period. A total of 1030 quadrats was collected from all 206 plots. The random plot data were established throughout Gannan Prefecture, according to grassland type and terrain conditions, and 291 plots were selected (Figure 1) during the grassland growth seasons from 2014 to 2016. Field survey plots were chosen to ensure a 5-km horizontal distance between plots and homogeneity of both vegetation and land use, and the geographical locations of the plots were selected to ensure that similar grassland types and geomorphology existed within a 250 m range around the plots, considering that MODIS pixels are 250 m × 250 m in size.

Grassland cover data were acquired from images collected by Phantom 2 vision+ (2014) and Phantom 3 professional (2015 and 2016) Quad-Rotor Intelligent UAVs, manufactured by DJI Industries (http://www.dji.com). The resolutions of the images collected by the two types of UAV are 1080 p (1920 × 1080) and 4 k (4000 × 3000), respectively. Both UAVs can automatically fly preset routes using a Naza-M autopilot system. The Phantom 2 vision+ UAV has a positional accuracy of ±2.5 m horizontally and ±0.8 m vertically. For the updated Phantom 3 professional version, the positional accuracy achieved is ±1.5 m horizontally and ±0.5 m vertically. The camera receives irradiance in the visible region (red, green, and blue spectral bands) and stores it as a digital number from 0 to 255 in JPEG format. The location information for each image is stored in its properties file. The UAVs were controlled to fly over each quadrat and took aerial photographs vertically downward at a height of approximately 30 m (the effective areas of the images were greater than 30 m × 30 m, and the actual resolution of the images was less than 2 cm; GPS information was acquired from the image properties file). Each image represented one quadrat, and grassland cover was calculated using a digital photo processing system (DPPS) [30]. Each plot corresponded to one remote-sensing pixel.

The flight paths of the UAVs were designed using FragMAP [31]. According to grassland growth status and spatial representativeness, the flight path was designed based on two routes: (1) if the grassland was relatively uniform and corresponded well to the remote-sensing pixel in the plot (as an example, one of the quadrats of the permanent sample plots is shown in Figure 2), the UAV took five photographs vertically downward at a height of approximately 30 m along one of the diagonal lines in the plot (maintaining an equal distance between each sample), after which the mean cover of the five quadrats was calculated as the plot cover; (2) if the grassland vegetation was complicated and distributed relatively non-uniformly, a square-shaped flight path (200 m × 200 m in area) was set for that plot (the geometric center of the square-shaped flight path corresponded to the MODIS pixel center); 12 photographs were then taken vertically downward at a height of approximately 30 m (Figure 1, Quadrats sample strategy), and the mean cover of the 12 quadrats was calculated as the plot cover.

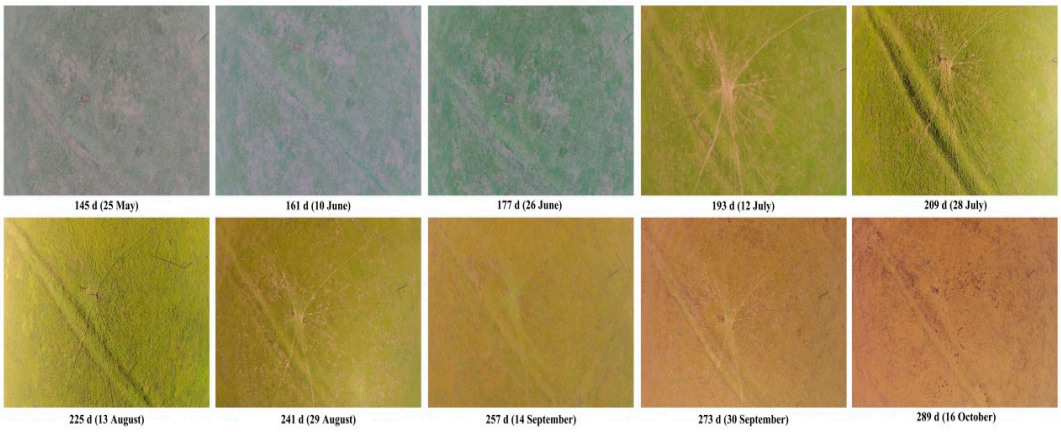

Figure 2. Digital photograph acquired by an unmanned aerial vehicle for one of quadrat of plot 7 in the permanent sample plot area in the growth season of 2015.

2.3. Soil, DEM and Meteorological Data

The DEM data employed were 90 m shuttle radar topography mission (SRTM) images (version V004) (http://srtm.csi.cgiar.org/) in Geo-TIFF format, resampled to 250 m in this study. The slope, topographic position index (TPI) and aspect were calculated based on the DEM. The soil data, including the sand and clay concentrations of the surface soil (0–30 cm) (represented as clay1 and sand1) and the bottom soil (30–60 cm) (represented as clay2 and sand2), were obtained from http://globalchange.bnu.edu.cn/research/soil [32]. The meteorological data, which consisted of a dataset with daily surface observation values for China (V 3.0), were acquired from the website of the China Meteorological Science Data Sharing Service (http://cdc.cma.gov.cn/). The daily temperature and precipitation data used in this study were obtained from 38 official meteorological stations in Gannan Prefecture and surrounding areas and cover the period from 2000 to 2016. The 16-day average temperature and cumulative precipitation data were calculated for each station according to the standard product synthesis date of MOD13Q1. Meteorological data (with 16-day temporal resolution) from outside stations were acquired through thin-plate smoothing spline (ANUSPLIN) interpolation [33,34]. Because the climate factor has a time lag effect on grassland cover [35,36], to explore the greatest correlation between the meteorological data and grassland cover, the differences in the time periods of the meteorological data were employed in this study.

The time corresponding to a field measurement (corresponding to the MOD13Q1 product data) was used as the current time (representing the 0-th period time), and the period of time before sampling was expressed as the i-th 16-day period (i for 1, 2, . . . , n, from the date back to 1 January and i up to a maximum value, n). We then tested the correlations between the meteorological data for all combinations of time periods and grassland cover, and the best-performing data were used to construct a model. The time periods are shown in Table 1.

Table 1. Combination of temperature and precipitation for each time period.

Time Period	1-th	2-th	3-th	. . .	*i*-th	. . .	*n*-th
1-th	0	0~1	0~2	. . .	0~$i-1$	. . .	0~$n-1$
2-th		1	1~2	. . .	1~$i-1$	. . .	1~$n-1$
3-th			2	. . .	2~$i-1$	. . .	2~$n-1$
. . .				. . .	3~$i-1$	. . .	3~$n-1$
i-th					. . .	. . .	...~$n-1$
. . .						. . .	$n-2$~$n-1$
n-th							$n-1$

For further analysis, the projection type of the DEM, soil and selected meteorological data was defined as Albers map projection. ArcGIS software was used to extract the value of each factor corresponding to the ground samples, and MATLAB software was employed for modeling and inversion.

2.4. MODIS Data and Preprocessing

The MODIS vegetation index data were selected from the MODIS 16-day maximum composite NDVI and EVI vegetation indices product (MOD13Q1) of the United States National Aeronautics and Space Administration. In total, 391 images with a spatial resolution of 250 m and orbit number, h26v05, were downloaded during the growth season of the grasslands (May to October) over a 17-year period (2000–2016). The MODIS reprojection tool (MRT) was employed to transform and register the MOD13Q1 NDVI and EVI data to the Albers map projection (Geo-Tiff format). The 16-day values of each of the vegetation indices for the study area as well as for the soil, DEM and meteorological data were then extracted for further analyses.

2.5. Construction of Grassland Cover Monitoring Models and Evaluation of Accuracy

2.5.1. Grassland Cover Monitoring Models

All data obtained using the above methods were employed to construct models for grassland cover during the grass growth season (May to October) using single-factor or multi-factor parametric and non-parametric regression models. (1): For the single-factor parametric regression models, the 14 variables included geographical location and topographical factors: longitude (X), latitude (Y), elevation (H), slope (S), aspect (A), and TPI; soil factors: sand1 (S1), clay1 (C1), sand2 (S2) and clay2 (C2); meteorological factors: 16-day average temperature (T) and cumulative precipitation (P) data; and MODIS vegetation indices: NDVI and EVI. These factors were used to construct the linear, exponential, logarithmic, power and separate regression models. (2): The variables of the multi-factor parametric models were selected by calculating their correlation with grassland cover. The multi-factor parametric regression models included multivariate linear and nonlinear models and are expressed as follows:

$$y = \beta_1 + \beta_2 x_1 + \beta_3 x_2 + \cdots + \beta_{i+1} x_i + u_i \quad (1)$$

$$y = \beta_1 + \beta_2 \ln x_1 + \beta_3 \ln x_2 + \cdots + \beta_{i+1} \ln x_i + u_i \quad (2)$$

$$y = A x_1^{\beta_1} x_2^{\beta_2} \cdots x_i^{\beta_i} e^{u_i} \quad (3)$$

$$y = \beta_1 + \beta_2 (1/x_1) + \beta_3 (1/x_2) + \cdots + \beta_{i+1} (1/x_i) + u_i \quad (4)$$

where y represents the grassland cover; x_1, x_2, $\cdots$, x_i are the variables selected based on showing a significant correlation with cover; β_1, β_2, $\cdots$, β_{i+1} are the model-fitting coefficients; and u_i represents the error term.

(3): The multi-factor non-parametric models employed in this study are artificial neural network (BP-ANN), support vector machine (SVM) and random forest (RF) models. The variables of these models are the same as for the multi-factor parametric models. The algorithms for the three models are as follows:

ANN is one of the most commonly used modeling methods based on gradient learning [37]. An ANN is a non-parametric nonlinear model that uses neural network spreading between layers and simulates human brain receivers and information processing [38]. The BP neural network refers to a multi-layer network structure consisting of an input layer, an output layer and one or more hidden layers. The Levenberg–Marquardt function algorithm was selected for ANN training in this study. The most important parameter in ANN regression models is the number of neurons and hidden layers; the greater the number of neurons and hidden layers, the higher the learning accuracy and the weaker the generalization ability. The network was designed to obtain an optimal topology. The numbers of hidden layers and neurons were determined based on a trial-and-error process [39]. In this study, the BP-ANN model and its validation were implemented using the MATLAB Neural Network toolbox.

SVM is a supervised learning model with associated learning algorithms, that analyzes data and performs pattern recognition and is also used in classification and regression analysis [40]. An SVM constructs a set of hyperplanes in high- or infinite-dimensional space, and these can be employed for classification, regression, and other tasks. Generally, the higher the functional margin, the lower the generalization error of the classifier. A regression version of SVM was proposed by Vapnik et al. [41]; in the present study, the radial basis function (RBF) was used as the kernel function, and the optimal cost and gamma values were obtained using the "Libsvm" package [42] in MATLAB.

The RF approach applies a set of decision trees to improve prediction accuracy, and the RF algorithm is based on the classification tree algorithm [43]. RF regression uses bootstrap sampling, and each bootstrap sample is employed to construct a decision tree. The training samples are constantly selected to minimize the sum of the squared residuals until a complete tree is formed. Multiple decision trees are formed, and voting is used to obtain the final prediction. The accuracy of the RF prediction depends on the regression trees; thus, an advantage of RF modeling is that it is not subject to over-fitting [44]. The model was established and validated using the RF function in the "RF_MexStandalone-v0.02" package within MATLAB.

2.5.2. Accuracy Evaluation

The performance of the aforementioned grassland cover estimation models was evaluated via 10-fold cross-validation [45,46], which ensured effective generalization [47]. The data sources (geographical location, topographical, soil and meteorological data and MODIS vegetation indices) were divided into 10 groups, each of which contained an approximately equal number of samples, for cross-validation. In each evaluation, except in the case of BP-ANN, 10% of the samples (1/10 of the total samples) were employed as a test set, and the remainder were used as the training set; for BP-ANN, 10% of the samples were used as the test set, another 10% of the samples were used as the validation set, and the remaining 80% made up the training set. R^2 and RMSE values were calculated for each dataset [48]. The process was repeated 10 times until each group had been employed as both a test set and as a training set (a validation set for BP-ANN). The model's performance is reflected by the mean R^2 and RMSE values obtained in the 10 runs. The model's stability is reflected by the standard deviation (SD) of the R^2 and the RMSE of the test set (denoted by SD_{R^2} and SD_{RMSE}). The higher the R^2 value, the smaller the RMSE, and the closer SD is to 0, the higher the precision, accuracy and stability of the model.

The formulae for R^2, RMSE and SD are as follows:

$$R^2 = \frac{SSE}{SST} = 1 - \frac{SSR}{SST} \tag{5}$$

$$SSR = \sum_{i=1}^{n} (cover_i - f_{cover}(i))^2 \tag{6}$$

$$SST = \sum_{i=1}^{n} (f_{cover}(i) - \overline{cover})^2 \tag{7}$$

$$RMSE = \sqrt{\frac{\sum_{i=1}^{n} (cover_i - f_{cover}(i))^2}{n}} \tag{8}$$

$$SD = \sqrt{\sum_{i=1}^{n} (x_i - \overline{x})^2 / N} \tag{9}$$

where SSR is the sum of squares due to regression, SST is the total sum of squares, $cover_i$ represents the i-th observed grassland cover, $\overline{cover}$ represents the mean value of the observed grassland cover, $f_{cover}(i)$ represents the i-th grassland cover estimated by the model, n represents the plots of the test set, x_i is the repeated R^2 and RMSE of the test set, $\overline{x}$ is the average value of x_i, and N is the number of modeling and validation repetitions.

2.6. Dynamic Variation and Trend Analysis

Based on the optimum grassland cover estimation model selected from the parametric and non-parametric regression models, the cover for days 145 to 289 (per 16 day) during each year was inverted, and the mean cover for a given day was calculated for the period, 2000 to 2016. Then, the dynamic variation in the grassland cover for the growth season in Gannan Prefecture was analyzed. In addition, the maximum grassland cover was calculated for the growth season cover during each year, and the dynamic variation trend of the maximum grassland cover was analyzed using the slope over the period 2000–2016 [3]. The formula for the slope is as follows:

$$slope = \frac{n \sum_{i=1}^{n} i \times cover_i - \sum_{i=1}^{n} i \sum_{i=1}^{n} cover_i}{n \times \sum_{i=1}^{n} i^2 - (\sum_{i=1}^{n} i)^2} \tag{10}$$

For further discussion of the spatial distribution pattern of grassland growth, the slope was categorized as significantly decreasing (<−0.6%/year), decreasing (−0.6–0.3%/year), stable (−0.3–0.3%/year), increasing (0.3–0.6%/year) or significantly increasing (>0.6%/year) [49–51].

3. Results and Analysis

3.1. Statistical Analysis of Observed Grassland Cover and Corresponding MODIS Vegetation Indices

Table 2 shows the statistical results obtained for grassland cover in the surveyed sample plots. NDVI and EVI were calculated using the corresponding remote-sensing data from 2014 to 2016. There were considerable differences in cover in the 497 sample plots in Gannan Prefecture during the grass growth season (May to September). In Gannan Prefecture, the average cover values ranged from 58.37% to 83.83% over the three-year period, and the coefficient of variation ranged from 0.17 to 0.43. The average NDVI and EVI ranged from 0.62 to 0.76 and from 0.40 to 0.58, respectively, with coefficients of variation ranging from 0.06 to 0.25 and from 0.09 to 0.31, respectively. In particular, the three highest average values of NDVI, EVI and cover were found in Maqu, Lintan and Luqu, respectively. For the entire prefecture, the average cover was 70.62% over the three-year period, with a CV of 0.37. The greatest grassland cover ranged from 1.38% to 99.87%. The maximum, minimum and average values of EVI (0.76, 0.14 and 0.47, respectively) were lower than those of NDVI (0.86, 0.28 and 0.67, respectively) overall. However, the degree of dispersion was similar; the SD of the two indices was 0.14, and the CVs were 0.30 and 0.20, respectively.

Table 2. Descriptive statistics of grassland cover and corresponding moderate-resolution imaging spectroradiometer (MODIS) normalized difference vegetation index (NDVI) and enhanced vegetation index (EVI) during May–September of 2014–2016 in the study area, Gannan Prefecture (n = 497).

Index	Statistical Indicator	Study Area							
		Zhuoni	Xiahe	Maqu	Lintan	Luqu	Hezuo	Diebu	All
NDVI	Maximum	0.71	0.86	0.85	0.76	0.85	0.80	0.75	0.86
	Minimum	0.62	0.28	0.43	0.68	0.56	0.45	0.52	0.28
	Average	0.67	0.62	0.76	0.72	0.72	0.66	0.63	0.67
	Standard deviation	0.05	0.14	0.08	0.04	0.08	0.12	0.16	0.14
	CV	0.07	0.22	0.11	0.06	0.11	0.19	0.25	0.20
EVI	Maximum	0.51	0.68	0.76	0.57	0.70	0.64	0.48	0.76
	Minimum	0.38	0.14	0.28	0.48	0.34	0.25	0.36	0.14
	Average	0.44	0.40	0.58	0.51	0.52	0.47	0.42	0.47
	Standard deviation	0.06	0.12	0.10	0.05	0.10	0.15	0.09	0.14
	CV	0.13	0.31	0.18	0.09	0.19	0.31	0.20	0.30
Cover	Maximum	94.75	99.83	99.87	91.31	98.01	96.28	85.64	99.87
	Minimum	33.07	1.38	18.66	58.43	33.01	26.72	67.52	1.38
	Average	58.37	63.36	83.83	78.61	75.49	67.12	66.58	70.62
	Standard deviation	27.39	27.67	17.98	17.67	18.87	25.89	12.81	25.99
	CV	0.47	0.44	0.21	0.22	0.25	0.39	0.17	0.37

3.2. Parametric Model Construction (Linear and Nonlinear) and Precision Evaluation

3.2.1. Single-factor Parametric Model

The results of the accuracy evaluation, validated through 10-fold cross-validation, for the single-factor parametric model based on the 14 variables (where the best-performing meteorological data are the 1st–4th precipitation and the 0th-2nd temperature data), are listed in Table 3. Using the 14 factors, four types of grassland cover estimation models (linear, logarithmic, power and exponential) based on MODIS EVI exhibited the best performance, showing the highest R^2 and lowest RMSE. These were followed by the NDVI, precipitation and temperature models. The performance of the other variables is shown in Table 2. Among the four types of estimation model, the logarithmic model based on EVI performed the best, with R^2 and RMSE of 0.52 and 16.96%, respectively; this model was followed by the NDVI, P, T, X, Y, H, S2, C1, S, C2, TPI and S1 models. The linear model based on A performed the worst, with R^2 and RMSE of 0.02 and 24.47%, respectively. Table 3 shows the parameters of the best-fitted model for each of the 14 variables. The EVI, NDVI, P, T, X, H, Y, C1 and S2 models pass the T test and the F test at significance levels of 0.001 or 0.05 (Table 4), but the other

models do not. Based on the model-fitted 10-fold cross-accuracy validation and optimum inversion models, the best-fitted models constructed based on each variable are listed in Table 5.

Table 3. Validation results obtained through 10-fold cross-validation for the grassland cover models based on a single factor.

Variable	Linear		Exponential		Logarithm		Power	
	R^2	RMSE	R^2	RMSE	R^2	RMSE	R^2	RMSE
EVI	0.49	17.39	0.46	17.06	0.52	16.96	0.50	17.37
NDVI	0.47	17.73	0.46	17.96	0.47	17.81	0.47	17.77
P	0.39	19.08	0.37	19.60	0.41	18.76	0.40	18.94
T	0.31	20.93	0.28	21.40	0.33	20.55	0.31	20.97
X	0.05	24.11	0.05	24.07	0.05	24.10	0.05	24.06
H	0.06	24.18	0.06	24.18	0.06	24.18	0.06	24.18
Y	0.05	24.16	0.05	24.15	0.05	24.16	0.05	24.14
C1	0.03	24.26	0.03	24.24	0.03	24.25	0.03	24.25
S2	0.05	24.20	0.05	24.20	0.05	24.19	0.05	24.19
S	0.03	24.37	0.03	24.37	-	-	-	-
C2	0.03	24.44	0.03	24.44	0.04	24.41	0.04	24.40
TPI	0.01	24.45	0.01	24.45	0.01	24.46	0.01	24.46
S1	0.02	24.46	0.02	24.46	0.02	24.48	0.02	24.48
A	0.02	24.47	0.02	24.47	-	-	-	-

Table 4. Results of model fitting with the optimum inversion models based on a single factor.

Vegetation Index	Parameter Estimation and *T* Test			Regression Significance Test	
	Parameter	Estimated Value	*T*	R^2	*F*
EVI	A	0.137	15.744 **	0.49	247.878 **
	B	−0.096	2.663 **		
NDVI	A	0.003	18.739 **	0.47	351.158 **
	B	0.470	39.395 **		
P	A	543.286	13.886 **	0.33	192.829 **
	B	−420.647	−2.577 *		
TAs	A	14.912	10.317 **	0.21	106.449 **
	B	48.217	7.996 **		
X	A	−0.001	−3.042 *	0.02	9.307 *
	B	102.771	698.162 **		
H	A	4.447×10^{-4}	3.506 **	0.03	12.292 **
	B	3175.107	107.046 **		
Y	A	−0.004	−2.568 *	0.02	6.596 *
	B	35.147	149.540 **		
C1	A	−0.001	−2.891 **	0.02	8.361 *
	B	17.914	32.479 **		
S2	A	1.236	2.086 *	0.01	4.352 *
	B	24.142	9.769 **		
S	A	−0.011	1.801	0.01	3.245
	B	2.956	6.526 **		
C2	A	−0.03	−1.285	1.644×10^{-3}	1.652
	B	22.334	9.628 **		
S1	A	0.004	0.324	2.658×10^{-4}	0.105
	B	31.515	39.366 **		
T	A	-4.889×10^{-4}	−0.281	1.993×10^{-4}	0.079
	B	4.104	31.991 **		
A	A	−0.006	−0.027	1.865×10^{-6}	0.001
	B	144.943	9.364 **		

Note: ** represents $p < 0.001$; * represents $p < 0.05$; A and B represent the constant and exponential term of the model, respectively; *T* and *F* are the significant values according to the *T* and *F* tests.

Table 5. Best fitted models constructed based on a single factor.

Variable	Formula	R^2
EVI	$y = 0.137\ln(x) - 0.096$	0.49
NDVI	$y = 0.003x + 0.470$	0.47
P	$y = 543.286\ln(x) - 420.647$	0.33
T	$y = 14.912\ln(x) + 48.217$	0.21
X	$y = -0.001x^{102.770}$	0.02
H	$y = 4.447\times10^{-4}e^{3175.107x}$	0.03
Y	$y = -0.004x^{35.147}$	0.02
C1	$y = -0.001e^{17.914x}$	0.04
S2	$y = 1.236\ln(x) + 24.142$	0.01

3.2.2. Multi-factor Parametric Model and Precision Evaluation

The results of the accuracy evaluation, validated through 10-fold cross-validation, for the multi-factor parametric models based on nine variables (selected from Section 3.2.1), are listed in Table 6. Among the four multi-factor parametric cover estimation models, the logarithmic model performed best, with an R^2 of 0.61 and an RMSE of 15.12%, followed by the linear model, with an R^2 of 0.60 and an RMSE of 15.39%, and then the reciprocal model. The power model exhibited the worst performance, with an R^2 of 0.58 and an RMSE of 15.70% (Table 6). Table 7 shows the parameters of the best-fitted model for each multi-factor parametric model. As shown, all four models passed the F test at a significance level of 0.001.

Table 6. Accuracy assessment of the different multi-factor parametric models using the 10-fold cross-validation method.

Model Forms	Training Set		Test Set	
	R^2	RMSE	R^2	RMSE
Linear	0.62	15.014	0.60	15.39
Logarithm	0.63	14.885	0.61	15.12
Power	0.60	15.523	0.58	15.70
Reciprocal	0.61	15.378	0.59	15.52

Table 7. Best fitted models constructed based on multiple factors.

Model Forms	Formula	R^2	*F*
Linear	$y = 361.0690 + 0.0247P - 0.1398T - 0.0648S2 - 0.0261H - 0.3031C1 - 6.7056X + 11.3646Y + 102.9434EVI + 23.7885NDVI$	0.62	71.01 **
Logarithm	$y = 2877.5978 + 36.8336\ln(P) - 12.7674\ln(T) + 1.5335\ln(S2) - 98.8390\ln(H) - 2.3321\ln(C1) - 700.1303\ln(X) + 299.7008\ln(Y) + 53.6374\ln(EVI) + 2.0236\ln(NDVI)$	0.63	73.04 **
Power	$y = 1.3840P^{0.5411}T^{-0.1455}S2^{0.0523}H^{-1.0555}C1^{0.0072}X^{-0.8194}Y^{3.7514}EVI^{0.6908}NDVI^{0.2119}$	0.60	58.99 **
Reciprocal	$y = -406.7349 - 2.9639\times10^4/P - 1.7307\times10^3/T - 147.3110/S2 + 1.7582\times10^5/H + 21.8384/C1 + 7.0831\times104/X - 6.2091\times10^3/Y - 17.1820/EVI - 8.4375/NDVI$	0.60	65.75 **

Note: ** represents $p < 0.01$; *F* are the significant values according to the *F* tests.

3.3. Multi-Factor Non-Parametric Regression Models Based on BP-ANN, SVM and RF and Evaluation of Precision

The results of the accuracy evaluation, validated through 10-fold cross-validation of the multi-factor non-parametric models, based on BP-ANN, SVM and RF, are listed in Table 8. The RF model performed best, with an R^2 of 0.78 and RMSE of 10.84%, whereas the accuracy of the BP-ANN model was lowest among the three models, with an R^2 of 0.72 and RMSE of 13.38%. The accuracy of the SVM model was between those of the RF and BP-ANN models, with an R^2 of 0.73 and RMSE of 12.83%.

Table 8. Accuracy assessment of the different multi-factor non-parametric regression models using the 10-fold cross-validation method.

Method	Training Set		Test Set	
	R^2	RMSE	R^2	RMSE
BP-ANN	0.83	10.288	0.72	13.38
SVM	0.90	7.804	0.73	12.83
RF	0.96	5.289	0.78	10.84

3.4. Comparison of Stability between Parametric and Non-Parametric Models (Optimum Inversion Model Selection)

The stability of a model with high accuracy is not necessarily high (Table 9). For the single-factor parametric models, $SD_R{}^2$ and SD_{RMSE} for EVI, NDVI, P and T showed lower stability at a higher accuracy. In contrast, the models based on X, H, Y, C1 and S2 exhibited higher stability, but the accuracy was lower. For multi-factor parametric models, the $SD_R{}^2$ and SD_{RMSE} of each model yielded similar values; the best stability was observed for the linear model (0.158 and 2.918% for $SD_R{}^2$ and SD_{RMSE}, respectively) and not for the logarithmic model, which displayed the best accuracy. For the multi-factor non-parametric models, $SD_R{}^2$ and SD_{RMSE} were the lowest for BP-ANN (0.062 and 1.615%, respectively), followed by SVM ($SD_R{}^2$ and SD_{RMSE} of 0.082 and 1.732%, respectively); the RF model showed poor stability, with $SD_R{}^2$ and SD_{RMSE} of 0.095 and 2.354%, respectively.

Comprehensively considering accuracy and stability, the BP-ANN model was the most suitable for describing the inversion of grassland cover in Gannan Prefecture.

Table 9. Performance of different models in the prediction of grassland cover.

Model	Factor	Function	$SD_R{}^2$	SD_{RMSE}
Single factor parametric models (including linear and nonlinear forms)	EVI	Logarithm	0.182	3.205
	NDVI	Linear	0.170	2.900
	P	Logarithm	0.171	2.689
	T	Logarithm	0.143	2.394
	X	Power	0.054	1.566
	H	Exponential	0.074	1.478
	Y	Power	0.062	1.595
	C1	Exponential	0.039	1.666
	S2	Logarithm	0.044	2.006
Multi-factor parametric models (including linear and nonlinear forms)	EVI, NDVI, P, T, X, H, Y, C1, S2	linear	0.158	2.918
		Logarithm	0.171	3.263
		Power	0.167	3.142
		Reciprocal	0.184	3.520
Multi-factor non-parametric models (nonlinear form)	EVI, NDVI, P, T, X, H, Y, C1, S2	BP-ANN	0.062	1.615
		SVM	0.082	1.732
		RF	0.095	2.354

3.5. Spatial and Temporal Dynamic Changes in Grassland Cover in Gannan Prefecture

3.5.1. Dynamic Changes During the Growth Season Every 16 day from 2000 to 2016

The distribution of average grassland cover during the growth season, from 2000 to 2016, was inverted by the BP-ANN model (Figure 3). Grassland cover presented a decreasing trend after increasing during the growth season. The growth season begins in May, and the average grassland cover can reach 41.74% at day 145 (25 May) in Gannan Prefecture (Figure 4). The regions showing the highest cover were the northwest, Xiahe, Luqu and Maqu; the maximum cover reached 91.63% in part of the study area. After the beginning of the growth season, grassland cover showed an increasing

trend from northwest to southeast until the day209 (28 July). The average grassland cover reached 78.61%, with cover ranging from 26.53% to 100%. The highest rate of increase of cover, 13.32%, occurred from day 177 to day 193. Grassland cover showed a decreasing trend from southeast to northwest after day 209 (28 July). The average cover was reduced to 58.59% at day 289 (16 October), although the highest-cover regions were still located in the northwest, Xiahe, Luqu and Maqu, and the maximum cover decreased to 95.05% in part of the study area.

The grassland cover first began to increase in Northwestern Gannan Prefecture and then gradually spread to the southeast during the growth season. After this first period of exuberance, the cover decreased from southeast to northwest. Compared with that in the southeast part of Gannan Prefecture, the growth season in the northwest, including Xiahe, Hezuo and Maqu, can be roughly estimated; because the beginning of the growth season there occurs earlier, and the end of the growth season occurs later—the growth season in the northwest is much longer.

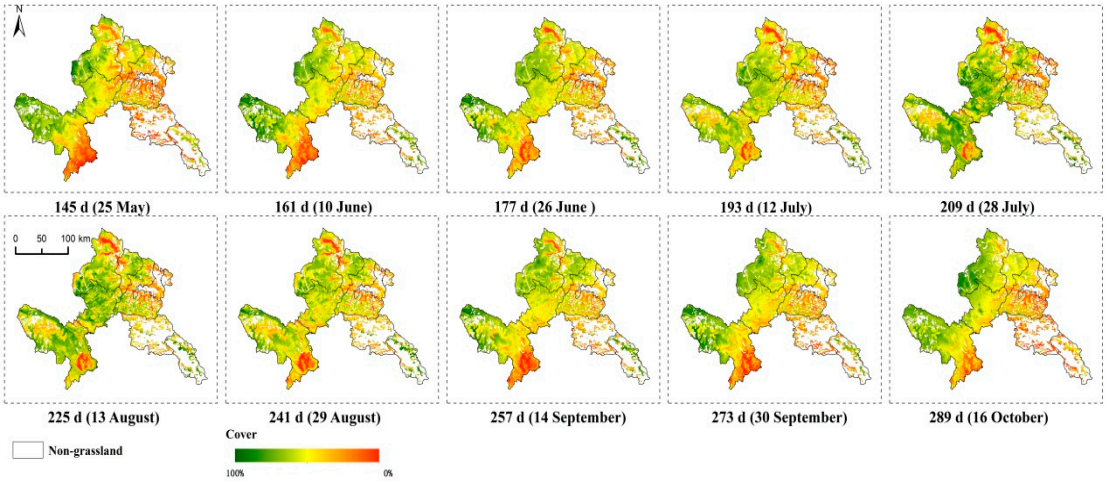

Figure 3. Spatial distribution of the average grassland cover for days 145–289 (per 16 days), on a pixel by pixel basis, in Gannan, from 2000 to 2016.

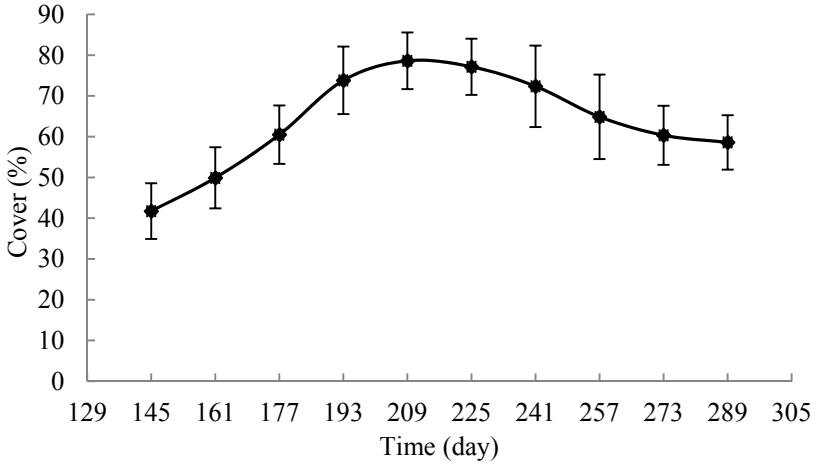

Figure 4. Spatial distribution of the average grassland cover for days 145–289 (per 16 days), in Gannan, from 2000 to 2016.

3.5.2. Dynamic Changes in Annual Maximum Grassland Cover

During the past 17 years, grassland cover has shown more increases than decreases (60.60% vs. 2.86%, respectively), with a stable area of 36.54% (Figure 5). The Northern (north of Xiahe) region of

Gannan Prefecture presented the most significant decrease (0.66%), while the Southern and central regions (south of Maqu and parts of Luqu, Zhuoni and Diebu) showed the most significant increases (27.86%). Cover decreased, but not significantly, in 2.2% of the study area, mostly in parts of Xiahe and Hezuo. Cover increased, but not significantly, in 32.74% of the study area, in parts of Lintan, Hezuo, Xiahe, Luqu and Maqu, outside of the significantly increasing areas shown in Figure 5.

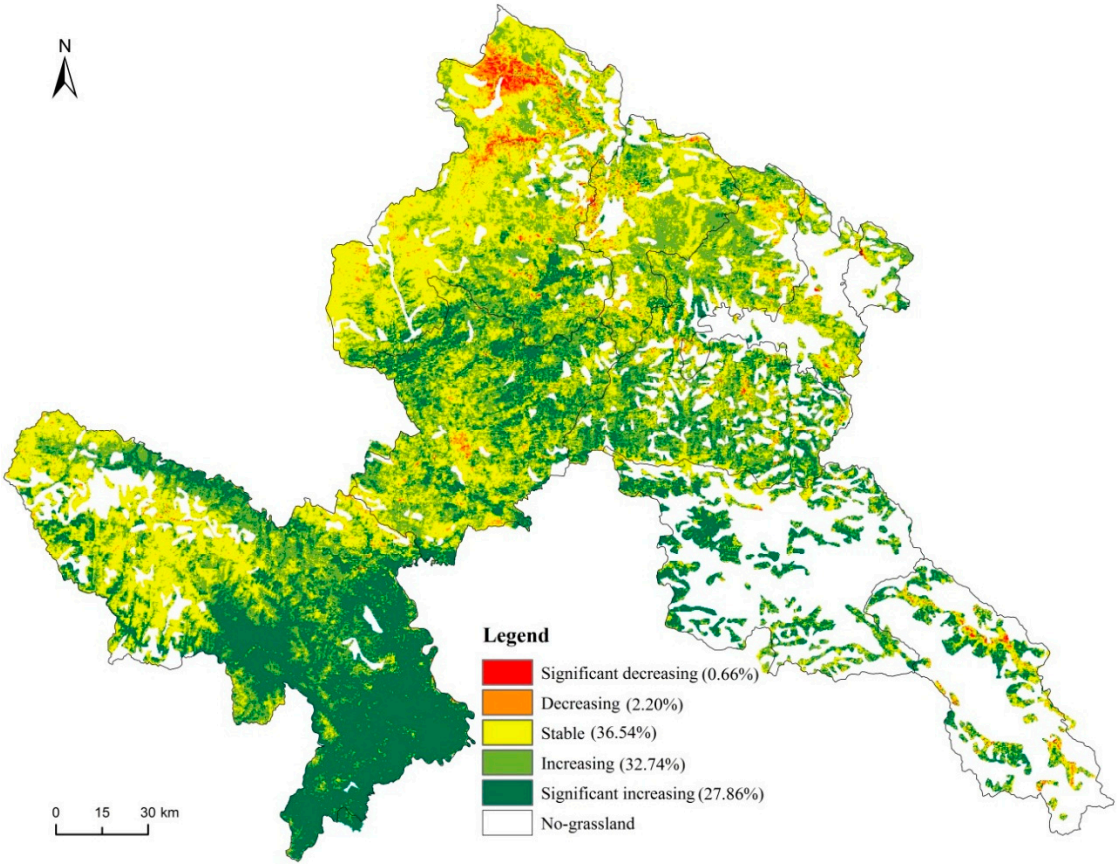

Figure 5. Variation of grassland cover in Gannan Prefecture from 2001 to 2016.

4. Discussion

4.1. Influence of Various Factors on Grassland Cover in Gannan Prefecture

In estimating grassland vegetation physical indices, multi-factor models are more reasonable than single vegetation indices (VI) obtained from remote sensing; single VI-based models exhibit low accuracy, poor stability, and considerable spatial variability across regions [2,3,52]. Previous research has indicated that topographic effects are not negligible when studying climatic impacts on vegetation in prairies with rolling topography [53]. Additionally, vegetation cover is indirectly influenced by soil texture [54], and grassland growth is strongly correlated with meteorological data [55–57].

Based on these considerations, geographical location and topographical factors (longitude, latitude, elevation, slope, aspect, and TPI), soil factors (sand1, clay1, sand2 and clay2), meteorological factors (temperature and precipitation data) and MODIS vegetation indices (NDVI and EVI) were considered in the present study to improve the accuracy of grassland cover estimation modeling from spatial resolution remote-sensing images. Grassland cover was extremely significantly ($p < 0.001$) correlated with the factors EVI, NDVI, P, T and H, with R^2 values ranging from 0.03 to 0.49, and was significantly ($p < 0.05$) correlated with the factors X, Y, C1 and S2, with R^2 of 0.01–0.02; no significant correlations were found for S, C2, S1, T or A. Remote-sensing vegetation indices were clearly the most effective indices for acquiring grassland cover directly, as found by Zhou et al. [49] and Li et al. [23],

and T, P and H exerted great influence on grassland vegetation cover estimation in the study area, similar to the findings of Yang et al. [58]. The effects of X, Y, C1 and S2 were smaller than those of the meteorological factors—S1, C2, S1, TPI and A—which had little influence on grassland cover. These results may be caused by the unique geographical location, terrain and climate of Gannan Prefecture [59]. For example, the elevation in this region gradually increases from east to west [60], the area exhibits a temperate plateau continental monsoon climate, with rain and heat occurring during the same period [56], and the grassland types are mostly alpine meadow and alpine shrub [4,59,60]. These selected factors are the same as those described in [2] and were employed to construct the above ground biomass model.

4.2. Comparative Analysis between Multi-Factor Parametric and Non-Parametric Models

In this study, models based on the field-observed cover data (measured by UAV) and the geographical location factors, topography, soil, meteorological data, and remote-sensing vegetation indices, including a single-factor parametric model and multi-factor parametric and non-parametric models, were analyzed. There were considerable differences among the models in accuracy and stability.

There was a significant difference in accuracy and stability between the single-factor parametric and multi-factor parametric inversion models. The higher-accuracy models showed lower stability than the single-factor parametric model. The accuracy of multi-factor parametric models was higher than that of the single-factor parametric models, showing an increase in R^2 of 0.09–0.60 and a decrease in RMSE of 0.19%–9.12%. However, the stability of the multi-factor parametric models was lower than that of the single-factor parametric models, with increases in $SD_R{}^2$ and SD_{RMSE} of 0.002–0.045 and 0.315%–2.042%, respectively. In contrast to the single-factor parametric and multi-factor parametric models, the multi-factor non-parametric models (including BP-ANN, SVM and RF) performed better in terms of accuracy and stability. With respect to accuracy, R^2 increased to 0.11–0.75 and RMSE decreased to 1.74%–13.41%. With respect to stability, $SD_R{}^2$ and SD_{RMSE} decreased to 0.089–0.122 and to 1.166%–1.905%, respectively. Among the three multi-factor non-parametric models, stability decreased as accuracy increased. The accuracy of the RF model was best (R^2 and RMSE values of 0.78 and 10.84%, respectively, compared with BP-ANN), but the stability of that model was low ($SD_R{}^2$ and SD_{RMSE} increased to 0.033 and 0.739%, respectively). In contrast, the lowest-accuracy model, BP-ANN, exhibited the highest stability.

Although the single-factor model is simple and easy to use [49], it showed lower accuracy and poor stability in this study. Previous work suggests that the estimation accuracy of a model can be improved by the use of multiple factors [2,3,61], but the stability of the model does not necessarily improve. For example, each of the multi-factor parametric models (linear, exponential, logarithmic, and power) exhibited high accuracy and low stability in this study. Because factor selection and expression are only conjecture, the single- and multi-factor parametric models are limited in some cases [1,62]. In this study, the best accuracy and stability overall were found for the multi-factor non-parametric models (including the BP-ANN, SVM and RF models). These models can estimate any complex nonlinear relationship and all the quantitative and qualitative information distributed within the models; thus, these models are robust and fault-tolerant [52,63].

4.3. Limitations and Prospects of a Model for Grassland Cover Monitoring in the Study Area

In this study, although the optimum models for the remote-sensing monitoring of grassland cover in the study area were determined, some error and uncertainty regarding these inversion models remain due to limitations associated with various factors.

4.3.1. Uncertainties in the Measured Data

Uncertainties in the measurements may be related to the degree of representativeness of a sample plot [4]; this factor is very important when calibrating model parameters and performing

validation [3]. Due to the limitations of GPS accuracy, topography, and traffic conditions, problems with representativeness are always encountered when matching sample plots to the corresponding pixels [64]. Although UAV technology was employed in this study to expand the sample plot area and reduce the influence of the heterogeneity of the land surface (this was accomplished by the use of 5–12 photographs representing each 250 m × 250 m area), heterogeneity could not be eliminated completely. The spatial representativeness of ground-sampling sites can be enhanced by increasing the number and area of quadrats, improving the range observed from the ground-sampling quadrats, and reducing the error from the corresponding spatial matching problem. Further sample settings are restricted by flight endurance (hovering time of the UAV), aircraft control distance, and the resolution of the photographs [16]. With the development of UAV science and technology, the sampling strategy still requires much improvement.

4.3.2. Temporal Matching Between Ground Sampling Sites and Remote-Sensing Data

Temporal disparities between the monthly maximum values of MODIS VIs and the field-measured biophysical parameters during the peak period of grass growth are unavoidable [65] despite experimenters' best efforts. In this study, data matching between the field-measured and remote-sensing VIs used data obtained within the shortest possible time intervals. In future research, the timing of field investigations should be planned to reduce the temporal disparity between field-measured biophysical parameters and satellite image acquisitions [4].

4.3.3. Limitations of the Optimum Estimation Model

Although the BP-ANN model exhibited high accuracy and was robust in this study, this model has obvious limitations. First, the accuracy of the learning process depends on the quantity and quality of the samples, and the convergence process can be slow or can suffer from problems of local minima. Second, as a black box method, the geometry of an ANN presents a complicated architecture, and the theoretical threshold for selecting a reasonable network structure is insufficient. Moreover, the over-fitting problem cannot be ignored when applying an ANN, and the optimal numbers of hidden layers and nodes depend on the problem itself and on repeated tests. In the end, the ANN model solves the problem related to the weight of network convergence, but it does not guarantee that the solution is optimal. Therefore, repeated training is required to obtain an optimal neural network and achieve reasonable results (for example, 10-fold cross-validation).

5. Conclusions

Based on an analysis of the factors influencing alpine grassland cover in the pastoral area of Gannan Prefecture, this study examined single-factor parametric and multi-factor parametric/non-parametric cover inversion models and evaluated their accuracy and stability. The dynamic variation in grassland cover was also analyzed. The following primary conclusions were reached.

Because of the complexity and extensive spatial distribution of natural grassland resources, grassland cover shows considerable spatial heterogeneity in the pastoral area of Gannan Prefecture, leading to substantial differences in the responses of MODIS EVI and NDVI to grassland cover. The average grassland cover ranged from 58.37% to 83.83% during the growth seasons in 2014 to 2016, corresponding to an average EVI and an average NDVI of 0.62–0.76 and 0.40–0.58, respectively. In particular, Maqu, Lintan and Luqu showed the maximum average values of cover, EVI and NDVI (0.51–0.58, 0.72–0.76, and 75.49%–83.83%, respectively).

Nine of the 14 examined factors presented significant correlations with grassland cover. EVI, NDVI, P, T, X, Y, H, C1 and S2 were significantly or extremely significantly correlated with grassland cover. Grassland cover inversion models based on a single factor exhibited poor accuracy and low stability. In the study area, EVI was most closely related to grassland cover, followed by NDVI, P, T, X, H, Y, S2 and C1. The single-factor grassland cover inversion models accounted for only 1%–49% of the variation in cover.

The multi-factor non-parametric models showed higher accuracy and stability than the single- and multi-factor parametric models. The accuracy of grassland cover inversion models based on multiple factors was higher than that of single-factor models. The multi-factor parametric models (linear, logarithmic, power and reciprocal) accounted for 60%–63% of the variation in cover, whereas the multi-factor non-parametric models accounted for 83%–96% of the variation. The stability of the parametric models was lower than that of the non-parametric models, with increases in $SD_R{}^2$ and SD_{RMSE} of 0.063–0.122 and 0.564%–1.905%, respectively. The optimum grassland cover inversion model was BP-ANN; it was selected through comprehensive consideration of model accuracy and stability, with an R^2, RMSE, $SD_R{}^2$ and SD_{RMSE} of 0.72, 13.38%, 0.062 and 1.615%, respectively.

Overall, the annual maximum grassland cover in Gannan Prefecture has shown an increasing trend over the past 17 years. The regions in which grassland cover increased accounted for 60.60% of the total study area, with 27.86% showing significant increases. The stable area of cover accounted for 36.54% of the total study area, with 2.86% of the area showing decreases and 0.66% of the area showing significant decreases.

Acknowledgments: This study was supported by the Program for Changjiang Scholars and Innovative Research Team in University (IRT_17R50), the National Natural Science Foundation of China (31672484, 31702175, and 41401472), the National Key Research and Development Program of China project (2017YFC0504801), and the 111 Project (B12002). We also appreciate the editor's and reviewers' constructive suggestions to greatly improve the paper.

Author Contributions: All authors contributed significantly to this manuscript. To be specific, Baoping Meng and Tiangang Liang designed this study. Baoping Meng, Jinglong Gao, Xia Cui, Jing Ge, Jianpeng Yin and Qisheng Feng were responsible for the data processing, analysis, and paper writing. Hongjie Xie made valuable revisions and editing of the paper.

Conflicts of Interest: The authors declare no conflict of interest.

References

1. Lehnert, L.W.; Meyer, H.; Wang, Y.; Miehe, G.; Thies, B.; Reudenbach, C.; Bendix, J. Retrieval of grassland plant coverage on the Tibetan Plateau based on a multi-scale, multi-sensor and multi-method approach. *Remote Sens. Environ.* **2015**, *164*, 197–207. [CrossRef]
2. Liang, T.; Yang, S.; Feng, Q.; Liu, B.; Zhang, R.; Huang, X.; Xie, H. Multi-factor modeling of above-ground biomass in alpine grassland: A case study in the Three-River Headwaters Region, China. *Remote Sens. Environ.* **2016**, *186*, 164–172. [CrossRef]
3. Yang, S.; Feng, Q.; Liang, T.; Liu, B.; Zhang, W.; Xie, H. Modeling grassland above-ground biomass based on artificial neural network and remote sensing in the three-river headwaters region. *Remote Sens. Environ.* **2017**, *204*, 448–455. [CrossRef]
4. Meng, B.; Ge, J.; Liang, T.; Yang, S.; Gao, J.; Feng, Q.; Cui, X.; Huang, X.; Xie, H. Evaluation of Remote Sensing Inversion Error for the Above-Ground Biomass of Alpine Meadow Grassland Based on Multi-Source Satellite Data. *Remote Sens.* **2017**, *9*, 372. [CrossRef]
5. Qin, X.; Sun, J.; Wang, X. Plant coverage is more sensitive than species diversity in indicating the dynamics of the above-ground biomass along a precipitation gradient on the Tibetan Plateau. *Ecol. Indic.* **2018**, *84*, 507–514. [CrossRef]
6. Feng, H.; Zou, B.; Luo, J. Coverage-dependent amplifiers of vegetation change on global water cycle dynamics. *J. Hydrol.* **2017**, *550*, 220–229. [CrossRef]
7. Hu, J.; Su, Y.; Tan, B.; Huang, D.; Yang, W.; Schull, M.; Bull, M.A.; Martonchik, J.V.; Diner, D.J.; Knyazikhin, Y.; Myneni, R.B. Analysis of the MISR LAI/FPAR product for spatial and temporal coverage, accuracy and consistency. *Remote Sens. Environ.* **2007**, *107*, 334–347. [CrossRef]
8. Dong, Y.; Lei, T.; Li, S.; Yuan, C.; Zhou, S.; Yang, X. Effects of rye grass coverage on soil loss from loess slopes. *Int. Soil Water Conserv. Res.* **2015**, *3*, 170–182. [CrossRef]
9. Hou, J.; Wang, H.; Fu, B.; Zhu, L.; Wang, Y.; Li, Z. Effects of plant diversity on soil erosion for different vegetation patterns. *Catena* **2016**, *147*, 632–637. [CrossRef]
10. Yao, X.; Yu, J.; Jiang, H.; Sun, W.; Li, Z. Roles of soil erodibility, rainfall erosivity and land use in affecting soil erosion at the basin scale. *Agric. Water Manag.* **2016**, *174*, 82–92. [CrossRef]

11. Gao, J.; Liu, Y.S. Determination of land degradation causes in tongyu county, northeast china via land cover change detection. *Int. J. Appl. Earth Obs. Geoinf.* **2010**, *12*, 9–16. [CrossRef]
12. Wang, P.; Deng, X.; Jiang, S. Diffused impact of grassland degradation over space: A case study in Qinghai province. *Phys. Chem. Earth-Parts A/B/C* **2017**, *101*, 166–171. [CrossRef]
13. Guo, S.M. Research of Vegetation Coverage Distribution Changes of Alpine Grassland Based on 3s Technology. Master's Thesis, Lanzhu University, Lanzhou, China, 2009.
14. Yi, S.; Zhou, Z.; Ren, S.; Xu, M.; Qin, Y.; Chen, S.; Ye, B. Effects of permafrost degradation on alpine grassland in a semi-arid basin on the Qinghai–Tibetan Plateau. *Environ. Res. Lett.* **2011**, *6*, 045403. [CrossRef]
15. Purevdorj, T.S.; Tateishi, R.; Ishiyama, T.; Honda, Y. Relationships between percent vegetation cover and vegetation indices. *Int. J. Remote Sens.* **1998**, *19*, 3519–3535. [CrossRef]
16. Chen, J.; Yi, S.; Qin, Y.; Wang, X. Improving estimates of fractional vegetation cover based on UAV in alpine grassland on the Qinghai–Tibetan Plateau. *Int. J. Remote Sens.* **2016**, *37*, 1922–1936. [CrossRef]
17. Maresma, Á.; Ariza, M.; Martínez, E.; Lloveras, J.; Martínez-Casasnovas, J. Analysis of Vegetation Indices to Determine Nitrogen Application and Yield Prediction in Maize (*Zea mays* L.) from a Standard UAV Service. *Remote Sens.* **2016**, *8*, 973. [CrossRef]
18. Holman, F.; Riche, A.; Michalski, A.; Castle, M.; Wooster, M.; Hawkesford, M. High Throughput Field Phenotyping of Wheat Plant Height and Growth Rate in Field Plot Trials Using UAV Based Remote Sensing. *Remote Sens.* **2016**, *8*, 1031. [CrossRef]
19. Yi, S.; Chen, J.; Qin, Y.; Xu, G. The burying and grazing effects of plateau pika on alpine grassland are small: A pilot study in a semiarid basin on the Qinghai-Tibet Plateau. *Biogeosciences* **2016**, *13*, 6273–6284. [CrossRef]
20. Chen, J.; Yi, S.; Qin, Y. The contribution of plateau pika disturbance and erosion on patchy alpine grassland soil on the Qinghai-Tibetan Plateau: Implications for grassland restoration. *Geoderma* **2017**, *297*, 1–9. [CrossRef]
21. Xu, B.; Yang, X.; Tao, W.; Qin, Z.; Liu, H.; Miao, J. Remote sensing monitoring upon the grass production in China. *Acta Ecol. Sin.* **2007**, *27*, 405–413. [CrossRef]
22. Göttlicher, D.; Obregón, A.; Homeier, J.; Rollenbeck, R.; Nauss, T.; Bendix, J. Land-cover classification in the andes of southern ecuador using landsat etm+ data as a basis for svat modelling. *Int. J. Remote Sens.* **2009**, *30*, 1867–1886. [CrossRef]
23. Li, T.; Li, X.; Li, F. Estimating Fractional Cover of Photosynthetic Vegetation and Non-photosynthetic Vegetation in the Xilingol Steppe Region with EO-1 Hyperion Data. *Shengtai Xuebao/Acta Ecol. Sin.* **2015**, *35*, 3643–3652.
24. Li, F.; Jiang, L.; Wang, X.; Zhang, X.; Zheng, J.; Zhao, Q. Estimating grassland aboveground biomass using multitemporal MODIS data in the West Songnen Plain, China. *J. Appl. Remote Sens.* **2013**, *7*, 073546. [CrossRef]
25. Diouf, A.A.; Hiernaux, P.; Brandt, M.; Faye, G.; Djaby, B.; Diop, M.B.; Ndione, J.A.; Tvchon, B. Do Agrometeorological Data Improve Optical Satellite-Based Estimations of the Herbaceous Yield in Sahelian Semi-Arid Ecosystems? *Remote Sens.* **2016**, *8*, 668. [CrossRef]
26. Yue, M.; Wei, F.Z. Based on energy evaluation for agricultural ecological system of Gannan Tibetan autonomous prefecture. *Res. Agric. Mod.* **2009**, *30*, 95–97.
27. Guo, Z.G.; Gao, X.H.; Liu, X.Y.; Liang, T.G. Ecological economic value and functions and classification management for grassland in Gannan prefecture, Gansu province. *J. Mt. Sci.* **2004**, *22*, 655–660.
28. Yang, Q.; Shi, H.M.; Ma, D.L.; Zhang, H.B.; Wen, G.Z.; Mu, Y.J.; Nian, M.X.; Zhao, J.; Bao, F.G. Observation on the adaptability of China grassland red cattle in southern Gansu area. *China Cattle Sci.* **2007**, *33*, 25–28.
29. Zhang, R.; Zhao, X.Y.; Zhao, H.L. Researching on the synthesis competitiveness in the high cold pasturing area—A case of Gannan Autonomy state. *J. Northwest Norm. Uni.* **2008**, *44*, 92–97.
30. Ren, S.L.; Shu-Hua, Y.I.; Chen, J.J.; Qin, Y.; Wang, X.Y. Comparisons of alpine grassland fractional vegetation cover estimation using different digital cameras and different image analysis methods. *Pratacult. Sci.* **2014**, *31*, 1007–1013.
31. Yi, S. FragMAP: A tool for long-term and cooperative monitoring and analysis of small-scale habitat fragmentation using an unmanned aerial vehicle. *Int. J. Remote Sens.* **2017**, *38*, 2686–2697. [CrossRef]
32. Wei, S.G.; Dai, Y.J.; Liu, B.Y.; Ye, A.Z.; Yuan, H. A soil particle-size distribution dataset for regional land and climate modelling in China. *Geoderma* **2012**, *171–172*, 85–91.

33. Zhang, R.; Liang, T.; Feng, Q.; Huang, X.; Wang, W.; Xie, H.; Guo, J. Evaluation and Adjustment of the AMSR2 Snow Depth Algorithm for the Northern Xinjiang Region, China. *IEEE J. Sel. Top. Appl. Earth Obs. Remote Sens.* **2017**, *10*, 3892–3903. [CrossRef]
34. McKenney, D.W.; Pedlar, J.H.; Papadopol, P.; Hutchinson, M.F. The development of 1901–2000 historical monthly climate models for Canada and the United States. *Agric. For. Meteorol.* **2006**, *138*, 69–81. [CrossRef]
35. Bao, Y.; Song, G.; Li, Z.; Gao, J.; Lü, H.; Wang, H.; Cheng, Y.; Xu, T. Study on the spatial differences and its time lag effect on climatic factors of the vegetation in the Longitudinal Range-Gorge Region. *Chin. Sci. Bull.* **2007**, *52*, 42–49. [CrossRef]
36. Zhou, W.; Gang, C.; Chen, Y.; Mu, S.; Sun, Z.; Li, J. Grassland coverage inter-annual variation and its coupling relation with hydrothermal factors in China during 1982–2010. *J. Geogr. Sci.* **2014**, *24*, 593–611. [CrossRef]
37. Yuan, H.; Yang, G.; Li, C.; Wang, Y.; Liu, J.; Yu, H.; Feng, H.; Xu, B.; Zhao, X.; Yang, X. Retrieving Soybean Leaf Area Index from Unmanned Aerial Vehicle Hyperspectral Remote Sensing: Analysis of RF, ANN, and SVM Regression Models. *Remote Sens.* **2017**, *9*, 309. [CrossRef]
38. He, Q. *Neural Network and its Application in IR*; Graduate School of Library and Information Science, University of Illinois at Urbana-Champaign Spring: Champaign, IL, USA, 1999.
39. Tiryaki, S.; Aydın, A. An artificial neural network model for predicting compression strength of heat treated woods and comparison with a multiple linear regression model. *Constr. Build. Mater.* **2014**, *62*, 102–108. [CrossRef]
40. Verrelst, J.; Camps-Valls, G.; Muñoz-Marí, J.; Rivera, J.P.; Veroustraete, F.; Clevers, J.G.P.W.; Moreno, J. Optical remote sensing and the retrieval of terrestrial vegetation bio-geophysical properties—A review. *ISPRS J. Photogramm. Remote Sens.* **2015**, *108*, 273–290. [CrossRef]
41. Vapnik, V.; Golowich, S.E.; Smola, A. Support vector method for function approximation, regression estimation, and signal processing. *Adv. Neur. Inf. Process. Syst.* **1997**, *9*, 281–287.
42. Chang, C.C.; Lin, C.J. *LIBSVM: A Library For Support Vector Machines*; ACM: New York, NY, USA, 2011.
43. Breiman, L. Random forests. *Mach. Learn.* **2001**, *45*, 5–32. [CrossRef]
44. Han, Z.Y.; Zhu, X.C.; Fang, X.Y.; Wang, Z.Y.; Wang, L.; Zhao, G.X.; Jiang, Y.M. Hyperspectral estimation of apple tree canopy LAI based on SVM and RF regression. *Spectrosc. Spectr. Anal.* **2016**, *36*, 800–805.
45. Jung, M.; Reichstein, M.; Margolis, H.A.; Cescatti, A.; Richardson, A.D.; Arain, M.A.; Arneth, A.; Bernhofer, C.; Bonal, D.; Chen, J.; et al. Global patterns of land–atmosphere fluxes of carbon dioxide, latent heat, and sensible heat derived from eddy covariance, satellite, and meteorological observations. *J. Geophys. Res. Biogeol.* **2011**, *116*, 245–255. [CrossRef]
46. Liu, Y.; Bi, J.W.; Fan, Z.P. Multi-class sentiment classification: The experimental comparisons of feature selection and machine learning algorithms. *Expert Syst. Appl.* **2017**, *80*, 323–339. [CrossRef]
47. Chou, J.S.; Pham, A.D. Nature-inspired metaheuristic optimization in least squares support vector regression for obtaining bridge scour information. *Inf. Sci.* **2017**, *399*, 64–80. [CrossRef]
48. Huang, J.C.; Gao, J.F. An ensemble simulation approach for artificial neural network: An example from chlorophyll a simulation in Lake Poyang, China. *Ecol. Inform.* **2017**, *37*, 52–58. [CrossRef]
49. Zhou, W.; Yang, H.; Huang, L.; Chen, C.; Lin, X.; Hu, Z.; Li, J. Grassland degradation remote sensing monitoring and driving factors quantitative assessment in China from 1982 to 2010. *Ecol. Indic.* **2017**, *83*, 303–313. [CrossRef]
50. Zhao, H.; Liu, S.; Dong, S.; Su, X.; Wang, X.; Wu, X.; Wu, L.; Zhang, X. Analysis of vegetation change associated with human disturbance using MODIS data on the rangelands of the Qinghai-Tibet Plateau. *Rang. J.* **2015**, *37*, 77. [CrossRef]
51. Dong, J.; Tao, F.; Zhang, G. Trends and variation in vegetation greenness related to geographic controls in middle and eastern Inner Mongolia, China. *Environ. Earth Sci.* **2010**, *62*, 245–256. [CrossRef]
52. Ali, I.; Cawkwell, F.; Dwyer, E.; Barrett, B.; Green, S. Satellite remote sensing of grasslands: From observation to management—A review. *J. Plant Ecol.* **2016**, *9*, 649–671. [CrossRef]
53. Li, Z.Q.; Guo, X.L. Topographic effects on vegetation biomass in semiarid mixed grassland under climate change using avhrr ndvi data. *Br. J. Environ. Clim. Chang.* **2014**, *4*, 229–242. [CrossRef] [PubMed]
54. Dodd, M.B.; Lauenroth, W.K.; Burke, I.C.; Chapman, P.L. Association between vegetation patterns and soil texture in the shortgrass steppe. *Plant Ecol.* **2002**, *158*, 127–137. [CrossRef]
55. Fang, J.; Yang, Y.; Ma, W.; Mohammat, A.; Shen, H. Ecosystem carbon stocks and their changes in China's grasslands. *Sci. China Life Sci.* **2010**, *53*, 757–765. [CrossRef] [PubMed]

56. Piao, S.; Fang, J.; Zhou, L.; Tan, K.; Tao, S. Changes in biomass carbon stocks in China's grasslands between 1982 and 1999. *Glob. Biogeochem. Cycl.* **2007**, *21*. [CrossRef]
57. Gao, T.; Yang, X.; Jin, Y.; Ma, H.; Li, J.; Yu, H.; Yu, Q.; Zheng, X.; Xu, B. Spatio-temporal variation in vegetation biomass and its relationships with climate factors in the Xilingol grasslands, Northern China. *PLoS ONE* **2013**, *8*, e83824. [CrossRef] [PubMed]
58. Yang, Y.H.; Piao, S.-L. Variations in grassland vegetation cover in relation to climatic factors on the tibetan plateau. *J. Plant Ecol.* **2006**, *30*, 1–8.
59. Cui, X.; Guo, Z.G.; Liang, T.G.; Shen, Y.Y.; Liu, X.Y.; Liu, Y. Classification management for grassland using MODIS data: A case study in the Gannan region, China. *Int. J. Remote Sens.* **2012**, *33*, 3156–3175. [CrossRef]
60. Ma, L.Y. Spatio-temporal dynamic changes of grassland vegetation cover and phenologg in Gannan prefecture. Master's Thesis, Lanzhu University, Lanzhou, China, 2013.
61. Feng, Y.; Cui, N.; Gong, D.; Zhang, Q.; Zhao, L. Evaluation of random forests and generalized regression neural networks for daily reference evapotranspiration modelling. *Agric. Water Manag.* **2017**, *193*, 163–173. [CrossRef]
62. Gao, T.; Xu, B.; Yang, X.; Jin, Y.; Ma, H.; Li, J.; Yu, H. Using MODIS time series data to estimate aboveground biomass and its spatio-temporal variation in Inner Mongolia's grassland between 2001 and 2011. *Int. J. Remote Sens.* **2013**, *34*, 7796–7810. [CrossRef]
63. Deo, R.C.; Sahin, M. Forecasting long-term global solar radiation with an ANN algorithm coupled with satellite-derived (MODIS) land surface temperature (LST) for regional locations in Queensland. *Renew. Sust. Energy Rev.* **2017**, *72*, 828–848. [CrossRef]
64. Yuan, X.L.; Li, L.H.; Tian, X.; Luo, G.P.; Chen, X. Estimation of above-ground biomass using MODIS satellite imagery of multiple land-cover types in China. *Remote Sens. Lett.* **2016**, *7*, 1141–1149. [CrossRef]
65. Eisfelder, C.; Kuenzer, C.; Dech, S. Derivation of biomass information for semi-arid areas using remote-sensing data. *Int. J. Remote Sens.* **2012**, *33*, 2937–2984. [CrossRef]